Model-Order Reduction of Finite-Element Approximations of Passive Electromagnetic Devices Including Lumped Electrical-Circuit Models

Hong Wu and Andreas C. Cangellaris, *Fellow, IEEE*

***Abstract*—A methodology is presented for the development of reduced-order macromodels for multiport passive electromagnetic devices that include embedded lumped elements. The proposed methodology utilizes a discrete state-space model for the electromagnetic device, generated through the application of the finite-element method for the spatial discretization of Maxwell's curl equations. The incorporation of lumped resistors, inductors, and capacitors is effected through the direct stamping of the state-space voltage–current relationship for these elements in the matrices of the generated state-space form of the discrete model. The conditions necessary for the discrete model to be passive are discussed. The subsequent reduction of the discrete state-space model is effected through the application of a Krylov-subspace-based model-order reduction scheme that guarantees the passivity of the generated multiport macromodel, provided that the original state-space model is passive. The proposed methodology is demonstrated and validated through its application for the generation of reduced-order macromodels for a coaxial cable circuit and a microstrip directional coupler circuit.**

***Index Terms*—Fast algorithms, finite-element methods (FEMS), full-wave computer-aided design (CAD), model-order reduction.**

I. Introduction

ACCURATE prediction of the electromagnetic response of integrated and packaged electronic components and systems is becoming of paramount importance as increasing switching speeds of digital electronics drive signal bandwidths to tens of gigahertz at all levels of packaging. This need is further compounded by the integration of sensitive RF and microwave components and functional blocks in close proximity with their noisy digital counterparts. Thus, in addition to supporting signal integrity and noise-aware digital signal and power distribution network design, computer-aided electromagnetic analysis becomes an indispensable tool for the prediction and mitigation of electromagnetic interference bottlenecks in mixed-signal integrated electronics.

Manuscript received December 15, 2003; revised June 1, 2004. This work was supported in part by Texas Instruments Incorporated under a custom research grant administered by the Semiconductor Research Corporation.

The authors are with the Center for Computational Electromagnetics and the Electromagnetics Laboratory, Department of Electrical and Computer Engineering, University of Illinois at Urbana-Champaign, Urbana, IL 61801 USA.

Digital Object Identifier 10.1109/TMTT.2004.834582

However, design-driven computer-aided electromagnetic analysis can be effective only if its computational efficiency can support expedient design iteration. For today's designs, the need for computational efficiency is driven primarily by short product design cycles. However, in the not very distant future, when virtual prototyping will be the only means for tackling the design challenges associated with first-pass design of mixed-signal and mixed-physics integrated microsytems and nanosystems, computationally efficient physics-based modeling and simulation will manifest itself as an indispensable enabling design capability.

Acknowledging the aforementioned modeling/simulation needs and technology trends, the computational electromagnetics community has been exploring numerous ways in which the escalating electromagnetic modeling complexity can be tackled effectively. These research efforts may be grouped in three classes. The first class involves fast integral-equation-based field solvers of computational complexity that scales linearly with the number of unknowns (e.g., [1]–[4]), and multigrid and multilevel methods for enhancing the robustness and expediting the convergence of finite-method-based solvers (e.g., [5]–[8], [18], and [19]).

The second class encompasses the various extensions of the model-order reduction techniques used extensively in large-scale circuit simulation ([9]–[12]) to the discrete model complexity reduction and subsequent compact macromodeling of electromagnetic structures in terms of broad-band multiport networks (e.g., [13]–[17], and [20]–[23]). In the context of finite-method-based discretization of electromagnetic systems, in addition to enhancing the efficiency of the numerical computation of the broad-band response of the electromagnetic device/component (e.g., [13]–[15], [17], and [21]–[23]), reduced-order macromodeling facilitates multiport electromagnetic device/component abstraction in matrix transfer function forms that are compatible with general-purpose linear and nonlinear network simulation tools (e.g., [16] and [20]). Furthermore, use of model-order reduction has been proposed as a means for facilitating and expediting finite-difference and finite-element modeling of structures containing multiple instantiations of the same feature or subcomponent, especially when its electrical size is small enough to require finer meshing for its discretization (e.g., [24]–[26]).

The third class of research efforts is concerned with the development of hybrid modeling methodologies, which, despite their limited investigation to date, hold the potential for significant improvement in both modeling versatility and computational efficiency compared to the methodologies in use today. Loosely speaking, hybrid methods are characterized by the concurrent utilization of different modeling methodologies and/or models, of different degrees of accuracy and complexity, to facilitate the development of comprehensive and accurate numerical models for electrically large and complicated structures.

A popular subset of the aforementioned hybrid models is the one that combines the application of a finite method (e.g., finite difference, finite element or finite volume) with lumped electrical-circuit elements for the modeling of high-frequency electromagnetic devices that exhibit significant disparity in the electrical size of their geometric features. One of the most common applications of such hybrid modeling has been in the electromagnetic analysis of integrated planar circuits, both passive and active (e.g., [27]–[33]). As a representative example, we mention the often considered in the literature model for integrated microwave amplifiers, where electromagnetic (distributed) models for the feed and matching networks are combined with lumped-circuit models for the semiconductor device, bond wires, and the terminating and biasing elements, the electrical size of which is sufficiently small to justify the use of lumped elements for their representation (see, e.g., [34]).

The recent trends for higher electronic functionality integration at the package and chip level will further increase the demand for the utilization of the aforementioned hybrid electromagnetic and lumped-circuit (EM–LC) modeling. The tight coupling of passive components in such three-dimensional environments renders the standalone modeling of individual components highly inaccurate, thus necessitating the implementation of comprehensive multicomponent models for accurate representation of the impact of component interactions on the electromagnetic response of the system. Furthermore, the geometric and material complexity of the three-dimensional multilayered geometries involved is such that finite methods are best suited for their modeling.

Once the electromagnetic analysis of the aforementioned EM–LC models has been completed, their abstraction in terms of broad-band multiport network representations, compatible with general-purpose network analysis-oriented nonlinear simulators is desired for the purposes of system-level analysis. A way in which the Krylov-subspace-based model-order reduction methods mentioned earlier can be applied for the development of such multiport representations of EM–LC models directly from the discrete model is presented in this paper.

This paper is organized as follows. The finite-element modeling methodology used is discussed first in Section II. The proposed Krylov-subspace-based model-order reduction methodology and its numerical implementation are discussed in Section III. This is followed by a presentation of several numerical studies in Section IV, aimed at the demonstration and validation of the proposed methodology. This paper concludes with a summary of the contributions of this study and a discussion of ongoing and future enhancements.

II. Finite-Element Model

A. Discretization of Maxwell's Curl Equations

The development of the finite-element model assumes a linear electromagnetic system. Even though the proposed model is applicable to the case of anisotropic media, material isotropy will be assumed for the purposes of this paper. Maxwell's curl equations in Laplace domain assume the form

$$\begin{aligned} \nabla \times \vec{E} &= -s\vec{B}, \\ \nabla \times \left(\frac{\vec{B}}{\mu}\right) &= s\epsilon\vec{E} + \sigma\vec{E} + \vec{J}_s \end{aligned} \tag{1}$$

where s is the complex frequency, (ϵ, μ, σ) denote the electromagnetic properties of the media (assumed to be position dependent), and $\vec{J}_s$ denotes the electric current source density. Following [35], the electric field intensity $\vec{E}$ and the magnetic flux density $\vec{B}$ are expanded, respectively, in the tangentially continuous vector space W_t and normally continuous vector space W_n. Hence, it is

$$\vec{E} = \sum_i^{N_e} x_{e_i}\vec{w}_{t_i} \quad \vec{B} = \sum_i^{N_b} x_{b_i}\vec{w}_{n_i}. \tag{2}$$

It is noted that, as it is immediately evident from the explicit forms of the expansion functions given in Section II-B, the units of $\vec{w}_{t_i}$ and $\vec{w}_{n_i}$ are, respectively, m^{-1} and m^{-2}. Hence, the coefficients in the expansions of $\vec{E}$ and $\vec{B}$ are, respectively, volts and webers. The above expansions will be used in the weak statement of the electromagnetic boundary value problem, which is obtained from (1) through multiplication of the first and second equations by $\mu^{-1}\vec{w}_{n_i}$ and $\vec{w}_{t_i}$, respectively, and subsequent integration over the domain of interest Ω with boundary S. After a straightforward integration by parts step, this yields

$$\begin{aligned} \int_\Omega \nabla \times \vec{E} \cdot \frac{1}{\mu}\vec{w}_n dv &= -s\int_\Omega \vec{B} \cdot \frac{1}{\mu}\vec{w}_n dv, \\ &\quad - \int_\Omega \nabla \times \vec{w}_t \cdot \frac{1}{\mu}\vec{B} dv \\ &\quad - \oint_S \hat{n} \times \vec{H} \cdot \vec{w}_t ds \\ &= -s\int_\Omega \epsilon\vec{E} \cdot \vec{w}_t dv \\ &\quad - \int_\Omega \sigma\vec{E} \cdot \vec{w}_t dv - \int_\Omega \vec{J}_s \cdot \vec{w}_t dv \end{aligned} \tag{3}$$

where $\hat{n}$ denotes the outward-pointing unit normal on S. For simplicity, only unbounded boundaries are considered for the purposes of this paper, on which the first-order absorbing boundary condition will be utilized for the purposes of this paper. Let η denote the intrinsic impedance of the unbounded medium. The first-order absorbing boundary condition then assumes the form

$$\hat{n} \times \vec{H} = \frac{1}{\eta}\hat{n} \times \hat{n} \times \vec{E}. \tag{4}$$

Substitution of (2) in (3) and subsequent testing with each one of the expansion functions $\vec{w}_{n_i}, i = 1, 2, \ldots, N_e$, and $\vec{w}_{t_i}, i =$

$1, 2, \ldots, N_b$ lead to the finite-element system of equations that may be cast in matrix form as follows:

$$\begin{bmatrix} 0 & D \\ -D^T & Z \end{bmatrix} \begin{bmatrix} x_b \\ x_e \end{bmatrix} = -s \begin{bmatrix} P_b & 0 \\ 0 & P_e \end{bmatrix} \begin{bmatrix} x_b \\ x_e \end{bmatrix} + \begin{bmatrix} 0 \\ u \end{bmatrix}. \quad (5)$$

The vectors x_b and x_e contain the expansion coefficients in the approximation of $\vec{B}$ and $\vec{E}$, respectively. The expressions for the elements of the matrices in (5) are given as follows:

$$\begin{aligned} D_{ij} &= \int_\Omega \nabla \times \vec{w}_{t_j} \cdot \frac{1}{\mu} \vec{w}_{n_i} dv \\ Z_{ij} &= \int_\Omega \vec{w}_{t_i} \cdot \sigma \vec{w}_{t_j} dv + \oint_S \hat{n} \times \vec{w}_{t_i} \cdot \frac{1}{\eta} \hat{n} \times \vec{w}_{t_j} d\vec{s} \\ P_{b_{ij}} &= \int_\Omega \vec{w}_{n_j} \cdot \frac{1}{\mu} \vec{w}_{n_i} dv \\ P_{e_{ij}} &= \int_\Omega \vec{w}_{t_i} \cdot \epsilon \vec{w}_{t_j} dv \\ u_i &= -\int_\Omega \vec{w}_{t_i} \cdot \vec{J}_s dv. \end{aligned} \quad (6)$$

This completes the discretization of Maxwell's curl equations. As discussed in detail in [17] and [35], in addition to physical consistency and improved numerical robustness, use of the tangentially continuous vector space W_t and normally continuous vector space W_n for the expansion of the electric-field intensity and the magnetic flux density, respectively, leads to the skew-symmetric matrix on the left-hand side of (5), a property needed to guarantee the passivity of the generated reduced-order macromodel of the electromagnetic system. This point will be elaborated further in Section II-B.

B. Incorporation of Lumped Elements

Next, the incorporation of lumped elements in the discrete model will be discussed. For this purpose, a specific choice for the order of the expansion functions is required. Thus, zeroth-order edge elements are chosen for the expansion of $\vec{E}$, accompanied by a consistent choice for the order of the expansion functions for $\vec{B}$, as follows:

$$\begin{aligned} \vec{w}_t \in W_t &= \{\lambda_i \nabla \lambda_j - \lambda_j \nabla \lambda_i \mid i < j\} \\ \vec{w}_n \in W_n &= \{\lambda_i \nabla \lambda_j \times \nabla \lambda_k + \lambda_j \nabla \lambda_k \times \nabla \lambda_i \\ &\quad + \lambda_k \nabla \lambda_i \times \nabla \lambda_j \mid i < j < k\}. \end{aligned} \quad (7)$$

In the above expression, λ_i are the simplex (or barycentric) coordinates [36]. Let k and k' denote two edges in the grid. $\vec{w}_t$ then satisfies the condition

$$\int_k' \vec{w}_{t_k} \cdot \vec{dl} = \delta_{k,k'} \quad (8)$$

where $\delta_{k,k'}$ is Kronecker's delta. This is the mathematical statement of the fact that the line integral of the edge element $\vec{w_{t_k}}$ in (7) equals 1 along the edge k and 0 along all others edges. This result facilitates the definition of the voltage V_k along edge k through the following integral:

$$V_k = \int_{\text{edge } k} \vec{E} \cdot \vec{dl} = \int_{\text{edge } k} \sum_i^{N_e} x_{e_i} \vec{w}_{t_i} \cdot \vec{dl} = x_{e_k}. \quad (9)$$

Furthermore, it enables the direct incorporation of a lumped current source in the discrete model in the following fashion. Let I_k denote a lumped current source to be inserted along edge k. Clearly, the electric current density source term must be used for its insertion in the electromagnetic model. Referring to the element expression for the source vector u in (5), it is

$$\begin{aligned} u_k &= -\int_\Omega \vec{w}_{t_k} \cdot \vec{J} dv \\ &= -\int_{\text{area}} \left(\int_{\text{edge k}} J \vec{w}_{t_k} \cdot \vec{dl} \right) ds \\ &= -I_k. \end{aligned} \quad (10)$$

Equations (9) and (10) suggest the following procedure for the incorporation of lumped resistors and lumped capacitors in the discrete model. The voltage–current relation for a resistor R is

$$R^{-1} V = I. \quad (11)$$

Hence, the insertion of a lumped resistor R_k at edge k can be effected through the addition of the term $R_k^{-1} x_{e_k}$ to the left-hand side of the second equation in (5). This yields

$$Z_{kk} \longrightarrow Z_{kk} + R_k^{-1}. \quad (12)$$

Similarly, using the fact that the voltage–current relation for a capacitor C is

$$sCV = I \quad (13)$$

the assignment of a lumped capacitor C_k at edge k is effected through the introduction of the term $sC_k x_{e_k}$ to the right-hand side of the second equation of (5). This yields

$$P_{e_{kk}} \longrightarrow P_{e_{kk}} + C_k. \quad (14)$$

The aforementioned procedure for the introduction of lumped resistors and capacitors in the discrete electromagnetic model could, in principle, also be used for the incorporation of lumped inductors. However, the voltage–current relation for the inductor, analogous to (11) and (13), involves the inverse of the complex frequency s

$$(sL)^{-1} V = I. \quad (15)$$

This form is not compatible with the linear in s form of (5), which lends itself to the utilization of Krylov-subspace-based model-order reduction processes. However, there is a simple way in which lumped inductors can be inserted in the discrete model without interfering with the Krylov model-order reduction process. The way this is done requires an understanding of the numerical process in which model-order reduction of (5) is implemented. Therefore, the incorporation of lumped inductors in the discrete electromagnetic model will be discussed in Section III in conjunction with the presentation of the proposed model-order reduction methodology.

III. Krylov Model-Order Reduction

In order to provide for a general multiple-input–multiple-output (MIMO) formalism of the model-order reduction

methodology, the source vector in (5) is rewritten in the following multiple-input form:

$$U_{(N\times 1)} = \begin{bmatrix} 0 \\ u \end{bmatrix} = \hat{T}_{(N\times M_p)} S_{(M_p\times 1)} = \begin{bmatrix} 0 \\ T \end{bmatrix}_{(N\times M_p)} S_{(M_p\times 1)}. \tag{16}$$

In (16), S denotes the vector of sources, where each one is assigned to one of the M_p ports of the system. The mapping matrix $\hat{T}$ maps the sources to the M_p edges of the finite-element mesh, along which the ports (and, hence, the sources) are assigned. N denotes the number of degrees of freedom in the finite-element approximation, which, in view of (2), is $N = N_e + N_b$.

Introducing the following matrix notation:

$$G = \begin{bmatrix} 0 & D \\ -D^T & Z \end{bmatrix} \quad C = \begin{bmatrix} P_b & 0 \\ 0 & P_e \end{bmatrix} \quad X = \begin{bmatrix} X_b \\ X_e \end{bmatrix} \tag{17}$$

the formal solution of (5) is given by

$$X = (G + sC)^{-1}\hat{T}S. \tag{18}$$

Since current sources are employed for the purposes of this formulation, a MIMO transfer function of the system can be obtained by sampling the voltage at the M_p ports. In view of (9) and (16), this is effected through the matrix operation

$$V_p = \hat{T}^T X = \left[\hat{T}^T (G + sC)^{-1}\hat{T}\right] S. \tag{19}$$

It is recognized immediately that the matrix

$$H_Z(s) = \hat{T}^T (G + sC)^{-1}\hat{T} \tag{20}$$

is the impedance matrix for the electromagnetic multiport.

A. Passive Model-Order Reduction

The model-order reduction process adopted for our purposes is the one introduced in [37]. Provided that the discrete system (5) is passive, it is shown in [37] that the generated reduced-order model is also passive. The passivity of (5) is, in turn, guaranteed provided that C is symmetric nonnegative definite and G is nonnegative definite. That C is symmetric nonnegative definite immediately follows from the expressions for the elements of the matrices P_b and P_e given in Section II, provided that the media have positive electric permittivity and magnetic permeability and that, in view of (14), the lumped capacitors are positive. With regards to G, it is shown in [37] that since G is skew symmetric, the matrix is nonnegative definite provided that Z is nonnegative definite. Clearly, from the expression for the elements of G, this is the case, provided that the conductivity of the media is nonnegative and that, in view of (12), the lumped resistors are nonnegative. In summary, (5) is a passive discrete model of the electromagnetic system; hence, application of the passive reduced-order interconnect macromdeling algorithm (PRIMA) model-order reduction process of [37] will result in a passive reduced-order model.

It has been pointed out repeatedly in the literature that all Krylov-subspace-based model-order reduction methods match a number of the moments of the transfer function at a predetermined frequency s_0 (e.g., [11] and [37]). The choice of s_0 is controlled by the frequency bandwidth over which the reduced-order model is desired to be accurate. Rewriting (20) in the form

$$H_Z(s) = \hat{T}^T\Big(I - (s - s_0)\big(-(G + s_0C)^{-1}C\big)\Big) \times (G + s_0C)^{-1}\hat{T} \tag{21}$$

leads to the definition of the following two matrices:

$$A_{(N\times N)} = -(G + s_0C)^{-1}C \tag{22}$$

$$R_{(N\times M_p)} = (G + s_0C)^{-1}\hat{T}. \tag{23}$$

These matrices are used for the construction of the Krylov subspace $K(A, R, q)$, where q denotes the order of the reduced model. The definition of the Krylov subspace given below indicates the procedure that is used for its construction

$$K(A, R, q) = \operatorname{colsp}\left[R, AR, A^2R, \ldots, A^{k-1}R, A^k r_0, A^k r_1, \ldots, A^k r_m,\right]$$
$$k = \left\lfloor \frac{q}{M_p} \right\rfloor, \qquad m = q - kM_p. \tag{24}$$

In the above equation r_n, $n = 1, 2, \ldots, M_p$ denotes the nth column of the matrix R.

Let $F_{(N\times M_p)}$ denote an orthonormal basis for $K(A, R, q)$. Through the use of the block Arnoldi algorithm, F is generated directly during the process of the construction of $K(A, R, q)$. The number of required iterations is $\lfloor q/M_p \rfloor + 1$. It is noted that the extra iteration is not required if the order q is an integer multiple of the number of ports M_p. The matrix F is used directly for the reduction of the original system through the following equations:

$$\begin{aligned} X &= F\tilde{X} \\ \tilde{T} &= F^H\hat{T} \\ \tilde{G} &= F^H G F \\ \tilde{C} &= F^H C F. \end{aligned} \tag{25}$$

In the above equation, $\tilde{X}$ is the reduced state vector and the superscript H denotes complex-conjugate matrix transposition.

B. Efficient Construction of F

As elaborated in [17], the computational efficiency of the construction of the Krylov subspace is penalized by the large dimension of the discrete electromagnetic problem. This, in turn, is due to the fact that, in the discrete model obtained from the discretization of Maxwell's curl equations, both the electric-field intensity and the magnetic flux density are kept as unknowns. A methodology for overcoming this bottleneck was proposed and demonstrated in [17]. This methodology is utilized for the purposes of the construction of the projection matrix F. Its key steps are presented in the development below. The reader is referred to [17] for a more detailed discussion.

First, it is noted that the computation of R can be split into two parts, i.e., a magnetic part R_b and an electric part R_e as follows:

$$R = (G + s_0C)^{-1}\hat{T} = \begin{bmatrix} R_b \\ R_e \end{bmatrix} = \begin{bmatrix} P_b^{-1}D & 0 \\ 0 & I \end{bmatrix} \begin{bmatrix} R_{bb} \\ R_e \end{bmatrix} \tag{26}$$

where it is

$$R_e = \left(D^T P_b^{-1} D + s_0 Z + s_0^2 P_e\right)^{-1} s_0 T$$
$$R_{bb} = \left(\frac{-1}{s_0}\right) R_e. \tag{27}$$

It is shown in [17] that the elements of the matrix $Y = D^T P_b^{-1} D$ are given by

$$Y_{ij} = \int_\Omega \nabla \times \vec{w}_{t_i} \cdot \frac{1}{\mu} \nabla \times \vec{w}_{t_j} dv. \tag{28}$$

At this point, it is appropriate to elaborate on the properties of the aforementioned matrix Y since its definition provides us with the means for incorporating lumped inductors in the discrete electromagnetic model. From (28), it is evident that the units of the elements of Y are $(\text{Henry})^{-1}$. This suggests that it is through Y that lumped inductors should be incorporated in the model.

Furthermore, from (5), it is immediately apparent that Y results from the elimination of the vector x_b. More specifically, this elimination results in the following matrix equation:

$$s^{-1} Y x_e + Z x_e + s P_e x_e = u. \tag{29}$$

Recognized as the finite-element approximation for the vector Helmholtz equation for the electric field [17], the physical interpretation of the three terms on the left-hand side of (29) is straightforward. Considering the equation associated with edge k in the finite-element mesh, with the forcing term on the right-hand side associated with an impressed current source along this edge and x_{e_k} representing the voltage along the edge, the three terms on the left-hand side are recognized, respectively, as the inductive, conductive, and capacitive components of the current flow through the edge. Consequently, in view of (15) and (9), it follows that the introduction of a lumped inductor L_k along the edge k can be effected through the addition of the quantity L_k^{-1} to the entry Y_{kk}. Hence, it is

$$Y_{kk} \longrightarrow Y_{kk} + L_k^{-1}. \tag{30}$$

Returning to the construction of the Krylov subspace, and recalling that in the block Arnoldi process the construction of the matrix F is effected directly during the Arnoldi iteration, F is also split into two parts, i.e., a magnetic part F_b and an electric part F_e. We define $F_{bb} = P_b^{-1} D F_b$. During the $p+1$ iteration step, it is then

$$\begin{aligned} F^{(p+1)} &= \begin{bmatrix} F_b^{(p+1)} \\ F_e^{(p+1)} \end{bmatrix} \\ &= \begin{bmatrix} P_b^{-1} D & 0 \\ 0 & I \end{bmatrix} \begin{bmatrix} F_{bb}^{(p+1)} \\ F_e^{(p+1)} \end{bmatrix} \\ &= A F^{(p)} \\ &= A \begin{bmatrix} P_b^{-1} D & 0 \\ 0 & I \end{bmatrix} \begin{bmatrix} F_{bb}^{(p)} \\ F_e^{(p)} \end{bmatrix}. \end{aligned} \tag{31}$$

$F_{bb}^{(p+1)}$ and $F_e^{(p+1)}$ are obtained through the equations

$$\begin{bmatrix} F_{bb}^{(p+1)} \\ F_e^{(p+1)} \end{bmatrix} = \begin{bmatrix} P_b^{-1} D & 0 \\ 0 & I \end{bmatrix}^{-1} A \begin{bmatrix} P_b^{-1} D & 0 \\ 0 & I \end{bmatrix} \begin{bmatrix} F_{bb}^{(p)} \\ F_e^{(p)} \end{bmatrix} \tag{32}$$

which can be written separately and explicitly as

$$\begin{aligned} F_e^{(p+1)} &= \left(Y + s_0 Z + s_0^2 P_e\right)^{-1} \left(s_0 P_e F_e^{(p)} + Y F_{bb}^{(p)}\right) \\ F_{bb}^{(p+1)} &= \left(\frac{-1}{s_0}\right) F_e^{(p+1)}. \end{aligned} \tag{33}$$

Clearly, the gain in efficiency stems from the fact that only the electric part for F is solved for (requiring the factorization of the matrix $\left(Y + s_0 Z + s_0^2 P_e\right)$ of dimension N_e. Similarly, the computation of the inner product in the Gramm–Schmidt orthogonalization step employed in the Arnoldi process can be approximated as follows:

$$\langle F_i, F_j \rangle \simeq \langle F_{e,i}, F_{e,j} \rangle \tag{34}$$

where use is made of the fact that the magnitude of the electric-field intensity $\vec{E}$ is much larger than the magnitude of the magnetic flux density $\vec{B}$. More specifically, it follows immediately from the differential equation statement of Faraday's law of induction that $|\vec{E}| \sim |sh||\vec{B}|$, where h stands for the finite-element grid size. In particular, it is the expansion frequency s_0 that dictates the relationship of $|\vec{E}|$ and $|\vec{B}|$ in the context of the Arnoldi process. Hence, it is the magnitude of the factor $w = |s_0 h|$ that controls the accuracy of the approximation (34). Expressed in terms of the wavelength λ_0 at the expansion frequency, it is $w = 2\pi v_p (h/\lambda_0)$, where v_p is the wave velocity. Clearly, the approximation (34) is expected to be highly accurate for the types of media encountered in most engineering applications provided that h/λ_0 does not become exceedingly small. For those cases where h/λ_0 is small enough to yield the approximation (34) inaccurate, the techniques of [7] and [8] must be applied instead for the solution of the finite-element approximation of the electromagnetic problem. This topic is beyond the scope of this paper, but will be addressed in a forthcoming paper.

Once F has been constructed, (25) is used to construct the reduced model. The equations for the matrix projections may be written in terms of F_e and F_{bb} as follows:

$$\begin{aligned} X = F\tilde{X} \Rightarrow \begin{bmatrix} \tilde{x}_b \\ \tilde{x}_e \end{bmatrix} &= \begin{bmatrix} P_b^{-1} D F_{bb} \tilde{x}_b \\ F_e \tilde{x}_e \end{bmatrix} \\ \tilde{G} = F^H G F &= F_{bb}^H Y F_e - F_e^H Y F_{bb} + F_e^H Z F_e \\ \tilde{C} = F^H C F &= F_{bb}^H Y F_{bb} + F_e^H P_e F_e \\ \tilde{T} = F^H \hat{T} &= F_e^H T. \end{aligned} \tag{35}$$

Finally, the impedance matrix representation for the reduced-order multiport system assumes the form

$$\tilde{H}_Z(s) = \tilde{T}^T (\tilde{G} + s\tilde{C})^{-1} \tilde{T}. \tag{36}$$

Each of the elements of $H_Z(s)$ is a rational function of s with q poles. The way these rational functions can be used in conjunction with general-purpose network analysis-oriented nonlinear

simulation tools has been discussed extensively in the literature (e.g., [9], [12], [16], and [37]).

IV. Numerical Experiments and Validation

The numerical examples presented here are for two structures for which (approximate) analytic solutions based on transmission-line (TL) theory can be obtained. This way, the proposed reduced-order macromodeling method can be validated.

A. Terminated Coaxial Cable

The first example considered is a terminated air-filled coaxial cable. The length of the coaxial cable is 1 m and its two electrodes are assumed to be perfectly conducting. The radius of the inner circular cylindrical electrode is 4 mm. The inner radius of the outer circular cylindrical electrode is 8 mm. The cable is terminated at its far end by a lumped circuit that includes a 100-pF capacitor in series with the parallel combination of a 5-Ω resistor with a 10-nH inductor. In addition, on the driving end of the cable, a 5-Ω shunt resistor is present connecting the two electrodes. A TL model for this system is straightforward to set up and analyze. For the purposes of macromodeling, what is of interest is the frequency-dependent input impedance of the resulting circuit.

The finite-element model for this structure is developed as follows. Since the two electrodes are perfectly conducting, only the cylindrical air-filled volume between them needs to be discretized. The two end surfaces of the cable are the ones used for the assignment of the lumped elements. Considering the far end first, two cascaded edges, connecting the inner and outer electrodes, are selected. The capacitor is assigned along one of these edges. The parallel combination of the resistor and inductor is assigned at the other edge. Along all the remaining edges on the far-end cross-sectional boundary surface, the perfect magnetic conductor (PMC) boundary condition is enforced. This is done to make the three-dimensional finite-element model for the structure mimic the TL model as closely as possible.

Similarly, on the cross-sectional boundary associated with the driving end of the coaxial cable, a PMC condition is assigned along all edges, except for one that connects the two electrodes, along which the 5-Ω resistor is assigned. This edge is also selected as the "port" at which the driving current source (of 1 A) will be connected and the voltage will be measured for obtaining the one-port input impedance of the terminated cable.

The bandwidth of interest is 600 MHz. The expansion frequency is taken to be 300 MHz. The finite-element model employed has 920 nodes and 3121 tetrahedra. The number of edge (electric field) unknowns is 2687, while the number of facet (magnetic flux) unknowns is 5617. Thus, the proposed methodology requires the LU decomposition (a procedure for decomposing a square matrix into a product of a lower triangular matrix and an upper triangular matrix) of a matrix of size 2687 instead of one of size 8304 that would be required if the modified Arnoldi process described in Section III was not implemented. The single-frequency LU decomposition of the sparse finite-element method (FEM) matrix requires 2 s on a Pentium IV (2.4 GHz) PC with 512-MB memory. The associated memory usage is 5 MB. Application of the PRIMA model-order reduction process for the generation of a macromodel of order 20 requires 0.5 s per iteration.

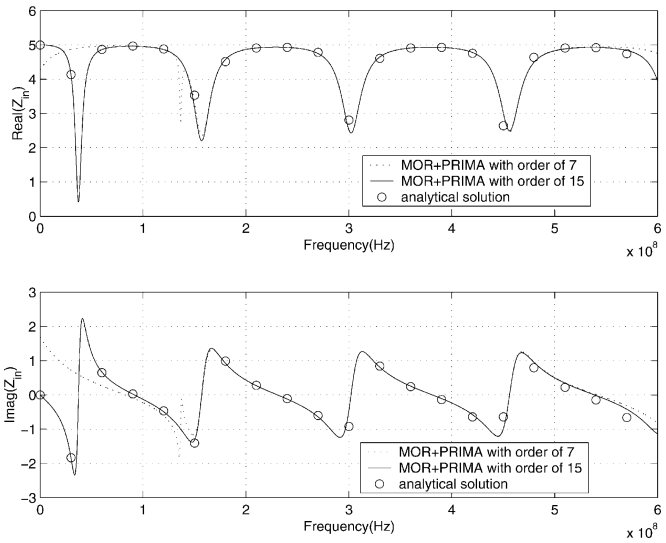

Fig. 1. Input impedance of a terminated coaxial cable.

The calculated real and imaginary parts of the input impedance are compared in Fig. 1 to those obtained from the analytical solution of the (approximate) TL model. For the case of a reduced model of order 7, a large deviation occurs below 150 MHz and above 550 MHz. Since the expansion frequency is taken at the middle point of the bandwidth of interest, (i.e., for this case, at 300 MHz), a degradation of the accuracy of the generated reduced-order model as we approach the end points of the bandwidth interval of interest is anticipated. This is indeed the case for the low-order reduced model. The situation is rectified by increasing the order of the reduced model. As indicated by the plots in Fig. 1, a reduced model of order 15 yields excellent accuracy across the entire bandwidth of interest.

B. Microstrip Directional Coupler

The second validation study conducted involved a microstrip directional coupler. While more complicated than the coaxial cable structure considered above, an analytic solution for the response of a directional coupler based on coupled TL theory is possible under the assumption that electromagnetic radiation and related higher-order electromagnetic effects associated with substrate mode excitation are neglected (e.g., [38]). However, the finite-element model for the structure will capture these effects; hence, a departure of the electromagnetic response obtained by the finite-element solution from that obtained using the TL model is to expected, especially at higher frequencies.

The strip dimensions for the coupler were selected such that both the characteristic impedance $Z_{\rm char}$ of the isolated microstrip and the quantity $\sqrt{Z_{\rm odd}Z_{\rm even}}$ (where $Z_{\rm odd}$, $Z_{\rm even}$ are, respectively, the odd- and even-mode impedances of the coupled symmetric microstrip) are 50 Ω. Thus, the strip width is 0.48 mm, the strip thickness is 0.1 mm, and the substrate thickness is 0.635 mm, while the edge to edge distance between the two strips is 0.43 mm. The relative permittivity of the substrate is 11.1. Both dielectric and conductor losses are

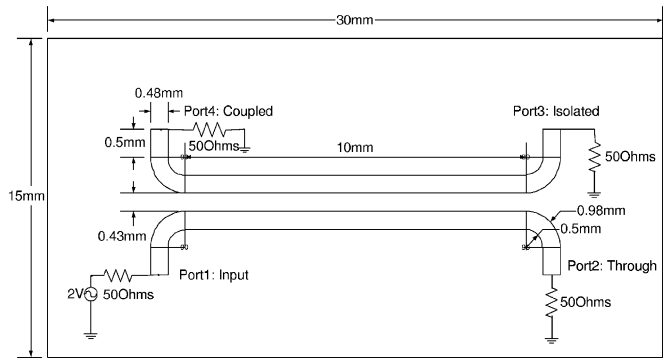

Fig. 2. Top view of the layout of the microstrip directional coupler.

assumed negligible for the purposes of this study. The length over which the two strips are coupled is taken to be 10 mm.

The geometry and material data described above suffice for the construction of the approximate TL model for the directional coupler. However, additional information is required for the completion of the three-dimensional geometry that will be analyzed using the FEM. Fig. 2 is provided to facilitate the description of the geometry. Four microstrip feed lines of length 0.5 mm and of the same cross-sectional dimensions with those of each strip, oriented normally to the axis of the coupler, are used to access the coupler. The transition from each feed line to the 10-mm-long coupled portion of the strips of the coupler is effected through 90° circular microstrip sectors of 0.5-mm inner radius and 0.98-mm outer radius. A 30 mm $\times$ 15 mm $\times$ 8 mm rectangular box is used as the computational domain for the finite-element modeling of the coupler. Except for the perfectly conducting bottom side that models the microstrip ground plane, the first-order absorbing boundary condition is imposed on the five remaining sides of the box to simulate an unbounded domain. The coupler geometry is placed in the center of the plane at a distance equal to the substrate thickness from the bottom side.

It is well known that the operation of the coupler requires 50-Ω (matched) terminations at its ports. This is done automatically in the finite-element model through the direct implementation of lumped 50-Ω resistors. The edges along which these resistors are connected serve as the ports for the resulting four-port structure. For the purposes of making a direct comparison with the results obtained from the approximate TL-based analysis of the coupler, the following excitation and termination scheme is employed. Port 1 is driven by a 2-V voltage source with a 50-Ω input resistance. In the finite-element model, this source is assigned along an edge that connects the strip to the ground. The remaining three ports are terminated with 50-Ω resistors, each resistor assigned to an edge that connects the strip to ground. (It should be clear that if a path of several cascaded edges is defined between a node on the strip and a node on the ground plane, the resistance value must be properly distributed among the edges so that the total resistance equals 50 Ω.) Finally, the port assignment is as follows. Port 2 is the through port at the far end of the driven line. Port 3 is the isolated port at the far end of the quiet line. Finally, Port 4 is the coupled port at the near end of the quiet line (directly opposite to the driven port).

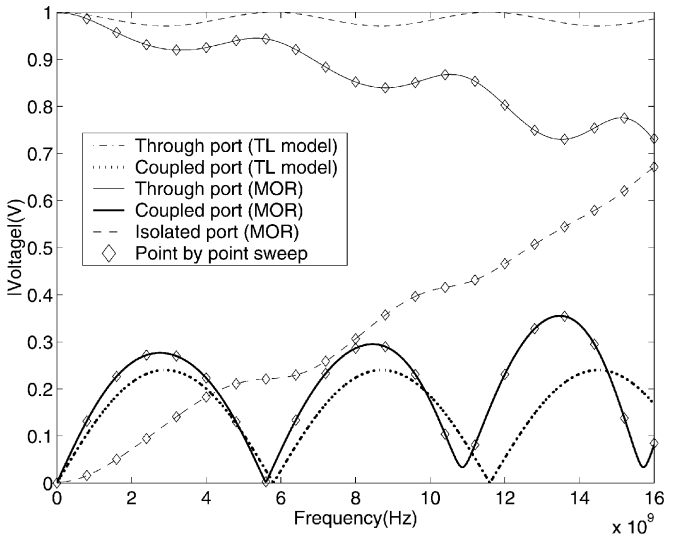

Fig. 3. Comparison of the responses obtained from the full-wave EM–LC model with those obtained from a coupled TL model for the microstrip directional coupler geometry of Fig. 2.

The number of edge (electric field) unknowns in the generated finite-element model is 59132, while the number of facet (magnetic flux) unknowns is 104 810. Thus, the proposed methodology requires the LU decomposition of a matrix of size 59 132 instead of one of size 163 942 that would be required if the modified Arnoldi process of Section III was not implemented. The expansion frequency was taken to be 8 GHz (i.e., at the center of the frequency band of interest). The single-frequency LU decomposition of the sparse FEM matrix requires 178 s on a Pentium IV (2.4 GHz) PC with 2-GB memory. The required memory is 750 MB. The CPU time for each iteration step in the Arnoldi process is approximately 10 s.

Fig. 3 depicts a comparison of the coupled TL model response for the coupler to that obtained from the finite-element-generated reduced-order model. The ideal behavior of total isolation and perfectly balanced power delivery to the coupled and through ports is clearly indicated over the 16-GHz frequency bandwidth of interest. The effective permittivity for the isolated microstrip is 6.69; hence, the 10-mm-long coupler is equal to $\lambda/4$ at a frequency of approximately 2.90 GHz. At this frequency, a peak for the voltage at the coupled port is expected in the analytic response. This is clearly confirmed from the plot in Fig. 3.

Also shown in Fig. 3 is the electromagnetic response obtained from the finite-element modeling of the actual three-dimensional structure. More specifically, both the response obtained through the solution of the problem at several frequencies over the bandwidth of interest, and the one generated by a reduced macromodel of order 20 are plotted. The two sets of responses are in excellent agreement. However, a discrepancy is observed between them and the ideal ones generated from coupled TL theory. Isolation of port 3 is not perfect anymore, and the coupling to it increases with frequency. Also increasing is the coupling to the coupled port. This increase in coupling for both ports is primarily due to the surface wave coupling through the substrate. As expected, this coupling comes at

the expense of a decrease in power received at the through port, as clearly depicted in Fig. 3. However, at sufficiently low frequencies, the calculated response correlates fairly well with the ideal response. For example, maximum coupling is obtained for a frequency very close to 2.90 GHz.

V. Concluding Remarks

In summary, a methodology has been presented and validated for the development of reduced-order macromodels of multiport passive electromagnetic devices that include lumped elements. The discrete electromagnetic model used in the model-order reduction process is obtained from the finite-element approximation of Maxwell's curl equations. Use of zeroth-order edge elements for the expansion of the electric-field intensity, accompanied by a consistent choice for the order of the expansion functions for the magnetic flux density, results in a passive discrete model, the state-space form of which facilitates the direct stamping of lumped elements such as resistors, inductors, capacitors, and lumped sources. Each of the lumped elements is assigned with an edge in the discrete finite-element model. Thus, the line integral of the electric field along the edge and the circulation of the magnetic field around the edge are used, respectively, as the associated voltage and current quantities for the lumped element. In this manner, in addition to modal ports, used previously for the purposes of macromodeling of electromagnetic devices, local ports can be defined, associated with either one or a set of cascaded edges in the grid.

The reduction of the generated discrete model is effected through the application of a modified version of a Krylov-subspace-based model-order reduction process called PRIMA. The modified version splits the construction of the Krylov subspace vectors into their electric-field intensity and magnetic flux density parts. In this manner, all matrix–vector product manipulations in the reduction process are associated with the calculation of the electric-field intensity only. The magnetic flux density is then calculated with $O(N)$ complexity through the discrete form of Faraday's law. Hence, the computational complexity of the model-order reduction process is controlled only by the number of edges in the finite-element model.

The proposed methodology and its numerical implementation were validated through their application for the modeling of structures for which approximate analytic solutions can be obtained using TL theory models. More specifically, a terminated coaxial cable and a symmetric microstrip directional coupler were analyzed.

Contrary to the traditional way in which network parameters for such waveguiding structures are generated (where the modal fields for the propagating modes at the waveguide ports are being used for the definition of the port variables), the incorporation of lumped-circuit elements in the model leads to increased flexibility in the way passive electromagnetic devices are modeled and multiport macromodels for them are defined.

For example, the direct incorporation of lumped-circuit element termination of waveguiding structures enables the more accurate modeling of higher-order electromagnetic attributes of these structures such as radiated emission and substrate-induced surface-wave excitation and coupling, and the incorporation of these effects in the generated reduced-order multiport network macromodel. Furthermore, combinations of resistive, capacitive, and inductive circuit elements are used to model lumped inductors or capacitors, often incorporated as surface-mounted components in both planar RF/microwave circuits (e.g., as tuning elements, RF chokes, or as elements of the bias circuit of active devices) and multilayered, interconnect, and power distribution networks for integrated and mixed-signal digital circuits (e.g., for decoupling and noise filtering). The proposed methodology facilitates the direct finite-element-based modeling and the subsequent reduced-order macromodeling of the resulting hybrid (distributed and lumped component) structures.

Building upon this concept of hybrid (distributed electromagnetic and lumped electrical circuit) modeling, the utilization of lumped-circuit element description of electrically small features of a complicated electromagnetic structure helps alleviate the finite-element grid construction and leads to discrete finite-element models with reduced number of unknowns. Such models are particularly useful in the analysis and reduced-order macromodeling of packaged, integrated RF/microwave, digital, and mixed-signal electronic systems. Methodologies for their systematic construction are currently under investigation and will be reported in a forthcoming paper.

Acknowledgment

The authors would like to thank Dr. Y. Zhu, Cadence Corporation, San Jose, CA, for helpful discussions pertinent to the finite-element modeling methodology used and the implementation of the model-order reduction algorithm.

References

[1] J. Zhao and W. C. Chew, "Integral equation solution of Maxwell's equations from zero frequency to microwave frequencies," *IEEE Trans. Antennas Propagat.*, vol. 48, pp. 1635–1645, Oct. 2000.

[2] V. I. Okhmatovski, J. Morsey, and A. C. Cangellaris, "Loop-tree implementation of the adaptive integral method (AIM) for numerically stable EM modeling from low to multi-GHz frequencies," in *Proc. IEEE Int. Antennas and Propagation Symp.*, vol. 1, June 22–27, 2003, pp. 11–14.

[3] M. Kamon, N. A. Marques, L. M. Silveira, and J. White, "Automatic generation of accurate circuit models of 3-D interconnect," *IEEE Trans. Comp., Pack., Manufact. Technol. B*, vol. 21, pp. 225–234, Aug. 1998.

[4] K. Aygun, B. Shanker, A. A. Ergin, and E. Michielssen, "A two-level plane wave time-domain algorithm for fast analysis of EMC/EMI problems," *IEEE Trans. Electromagn. Compat.*, vol. 44, pp. 152–164, Feb. 2002.

[5] D.-K. Sun, J.-F. Lee, and Z. Cendes, "Construction of nearly orthogonal nedelec bases for rapid convergence with multilevel preconditioned solvers," *SIAM J. Sci. Comput.*, vol. 23, no. 4, pp. 1053–1076, 2001.

[6] R. Dyczij-Edlinger, G. Peng, and J.-F. Lee, "Efficient finite element solvers for the Maxwell equations in the frequency domain," *Comput. Methods Appl. Mech. Eng.*, vol. 169, no. 3–4, pp. 297–309, Feb. 1999.

[7] Y. Zhu and A. C. Cangellaris, "Hierarchical multilevel potential preconditioner for fast finite-element analysis of microwave devices," *IEEE Trans. Microwave Theory Tech.*, vol. 50, pp. 1984–1989, Aug. 2002.

[8] ——, "Hybrid multilevel/multigrid potential preconditioner for fast finite element modeling," *IEEE Microwave Wireless Comp.*, vol. 12, pp. 290–292, Aug. 2002.

[9] E. Chiprout and M. S. Nakhla, *Asymptotic Waveform Evaluation and Moment Matching for Interconnect Analysis*. Boston, MA: Kluwer, 1993.

[10] P. Feldmann and R. W. Freund, "Efficient linear circuit analysis by Padé approximation via the Lanczos process," *IEEE Trans. Computer-Aided Design*, vol. 14, pp. 639–649, May 1995.

[11] R. W. Freund, "Passive reduced-order modeling via Krylov-subspace methods," in *IEEE Int. Computer-Aided Control System Design Symp.*, Sept. 2000, pp. 261–266.
[12] M. Celik, L. Pileggi, and A. Odabasioglu, *IC Interconnect Analysis*. Boston, MA: Kluwer, 2002.
[13] J. E. Bracken, D.-K. Sun, and Z. J. Cendes, "S-domain methods for simultaneous time and frequency characterization of electromagnetic devices," *IEEE Trans. Microwave Theory Tech.*, vol. 46, pp. 1277–1290, Sept. 1998.
[14] X.-M. Zhang and J.-F. Lee, "Application of the AWE method with the 3-D TVFEM to model spectral responses of passive microwave components," *IEEE Trans. Microwave Theory Tech.*, vol. 46, pp. 1735–1741, Nov. 1998.
[15] A. C. Cangellaris and L. Zhao, "Rapid FDTD simulation without time stepping," *IEEE Microwave Guided Wave Lett.*, vol. 9, pp. 4–6, Jan. 1999.
[16] A. C. Cangellaris, M. Celik, S. Pasha, and L. Zhao, "Electromagnetic model order reduction for system-level modeling," *IEEE Trans. Microwave Theory Tech.*, vol. 47, pp. 840–850, June 1999.
[17] Y. Zhu and A. C. Cangellaris, "A new finite element model for reduced order electromagnetic modeling," *IEEE Microwave Wireless Comp. Lett.*, vol. 11, pp. 211–213, May 2001.
[18] R. Dyczij-Edlinger, G. Peng, and J.-F. Lee, "Efficient finite element solvers for the Maxwell equations in the frequency domain," *Comput. Methods Appl. Mech. Eng. (Special Issue)*, vol. 169, no. 3–4, pp. 297–309, Feb. 1999.
[19] D. K. Sun, J. F. Lee, and Z. J. Cendes, "Construction of nearly orthogonal nedelec bases for rapid convergence with multilevel preconditioned solvers," *SIAM J. Sci. Comput.*, vol. 23, no. 4, pp. 1053–1076, 2001.
[20] D.-K. Sun, Z. Cendes, and J.-F. Lee, "ALPS-A new fast frequency-sweep procedure for microwave devices," *IEEE Trans. Microwave Theory Tech.*, vol. 49, pp. 398–402, Feb. 2001.
[21] T. Wittig, I. Munteanu, R. Schuhmann, and T. Weiland, "Two-step Lanczos algorithm for model order reduction," *IEEE Trans. Magn.*, vol. 38, pp. 673–676, Mar. 2002.
[22] L. Knockaert and D. De Zutter, "Stable Laguerre–SVD reduced-order modeling," *IEEE Trans. Circuits Syst. I*, vol. 50, pp. 576–579, Apr. 2003.
[23] D. Lukashevich, A. Cangellaris, and P. Russer, "Transmission line matrix method reduced order modeling," in *IEEE MTT-S Int. Microwave Symp. Dig.*, vol. 2, June 2003, pp. 1125–1128.
[24] Y. Zhu and A. C. Cangellaris, "Macro-elements for efficient FEM simulation of small geometric features in waveguide components," *IEEE Trans. Microwave Theory Tech.*, vol. 48, pp. 2254–2260, Dec. 2000.
[25] B. Denecker, F. Olyslager, L. Knockaert, and D. De Zutter, "Generation of FDTD subcell equations by means of reduced order modeling," *IEEE Trans. Antennas Propagat.*, vol. 51, pp. 1806–1817, Aug. 2003.
[26] L. Kulas and M. Mrozowski, "Reduced order models of refined Yee's cells," *IEEE Microwave Wireless Comp. Lett.*, vol. 13, pp. 164–166, Apr. 2003.
[27] P. B. Johns and M. O'Brien, "Use of transmission line modeling (T.L.M.) method to solve nonlinear lumped networks," *Radio Electron. Eng.*, vol. 50, no. 1–2, pp. 59–70, Jan.–Feb. 1980.
[28] R. H. Voelker and R. J. Lomax, "A finite-difference transmission line matrix method incorporating a nonlinear device model," *IEEE Trans. Microwave Theory Tech.*, vol. 38, pp. 302–312, Mar. 1990.
[29] W. Sui, D. A. Christensen, and C. H. Durney, "Extending the two-dimensional FDTD method to hybrid electromagnetic systems with active and passive lumped elements," *IEEE Trans. Microwave Theory Tech.*, vol. 40, pp. 724–730, Apr. 1992.
[30] Y.-S. Tsuei, A. C. Cangellaris, and J. L. Prince, "Rigorous electromagnetic modeling of chip-to-package (first-level) interconnections," *IEEE Trans. Comp., Hybrids, Manufact. Technol.*, vol. 16, pp. 876–883, Dec. 1993.
[31] M. Piket-May, A. Taflove, and J. Baron, "FD-TD modeling of digital signal propagation in 3-D circuits with passive and active loads," *IEEE Trans. Microwave Theory Tech.*, vol. 42, pp. 1514–1523, Aug. 1994.
[32] K. Guillouard, M.-F. Wong, V. F. Hanna, and J. Citerne, "A new global finite element analysis of microwave circuits including lumped elements," *IEEE Trans. Microwave Theory Tech.*, vol. 44, pp. 2587–2594, Dec. 1996.
[33] M. Feliziani and F. Maradei, "Modeling of electromagnetic fields and electrical circuits with lumped and distributed elements by the WETD method," *IEEE Trans. Magn.*, vol. 35, pp. 1666–1669, May 1999.
[34] S.-H. Chang, R. Coccioli, Y. Qian, and T. Itoh, "A global finite-element time-domain analysis of active nonlinear microwave circuits," *IEEE Trans. Microwave Theory Tech.*, vol. 47, pp. 2410–2416, Dec. 1999.
[35] Y. Zhu and A. Cangellaris, "Hierarchical finite element basis function spaces for tetrahedra elements," presented at the Applied Computational Electromagnetics Soc. Meeting, Monterey, CA, Mar. 2001.
[36] P. P. Silvester and R. L. Ferrari, *Finite Elements for Electrical Engineers*, 3rd ed. Cambridge, U.K.: Cambridge Univ. Press, 1996.
[37] A. Odabasioglu, M. Celik, and L. T. Pileggi, "PRIMA: Passive reduced-order interconnect macromodeling algorithm," *IEEE Trans. Computer-Aided Design*, vol. 17, pp. 645–654, Aug. 1998.
[38] D. M. Pozar, *Microwave Engineering*. Reading, MA: Addison-Wesley, 1990, ch. 8.

Hong Wu received the B.S. degree in computational mathematics from Nanjing University, Nanjing, China, in 2002, and is currently working toward the Ph.D. degree in electrical and computer engineering at the University of Illinois at Urbana-Champaign.

Since 2002, he has been a Research Assistant with the Center for Computational Electromagnetics, University of Illinois at Urbana-Champaign. His research interest is FEMs for electromagnetic modeling of integrated RF and high-speed digital circuits.

Andreas C. Cangellaris (M'86–SM'96–F'00) received the Diploma degree in electrical engineering from the Aristotle University of Thessaloniki, Thessaloniki, Greece, in 1981, and the M.S. and Ph.D. degrees in electrical and computer engineering from the University of California at Berkeley, in 1983 and 1985, respectively.

He is Professor of electrical and computer engineering at the University of Illinois at Urbana Champaign (UIUC). Prior to joining UIUC, he was on the faculty of Electrical and Computer Engineering, University of Arizona, initially as an Assistant Professor (1987–1992) and then as an Associate Professor (1992–1997). Prior to that, he was a Senior Research Engineer with the Electronics Department, General Motors Research Laboratories, Warren, MI (1985–1987). Over the past 17 years, he has supervised the development of electromagnetic modeling methodologies and numerous computer modeling and simulation tools for high-speed/high-frequency signal integrity-driven applications, which have been transferred successfully to industry. He has coauthored over 200 refereed papers and conference proceedings papers, as well as three book chapters on topics related to computational electromagnetics and the electrical performance analysis and optimization of the signal and power distribution network in high-speed/high-frequency integrated electronic systems. His research has been in the areas of applied and computational electromagnetics with emphasis on their application to electrical modeling and simulation of RF/microwave components and systems, high-speed digital interconnects at the board, package, and chip level, and the modeling and simulation of electromagnetic compatibility and electromagnetic interference in integrated electronic subsystems and systems.

Prof. Cangellaris is an active member of the IEEE Microwave Theory and Techniques Society (IEEE MTT-S), the IEEE Components Packaging and Manufacturing Technology Society, the IEEE Antennas and Propagation Society (IEEE AP-S), and the IEEE Magnetics Society. He serves as member of Technical Program Committees for major conferences and symposia sponsored by these societies. He has served as associate editor for the IEEE TRANSACTIONS ON ANTENNAS AND PROPAGATION. He is currently serving as associate editor of the IEEE TRANSACTIONS ON ADVANCED PACKAGING, the IEEE TRANSACTIONS ON MICROWAVE THEORY AND TECHNIQUES, and the IEEE Press Series on "Electromagnetic Fields and Waves." He is the co-founder of the IEEE Topical Meeting on Electrical Performance of Electronic Packaging.